AD_____

Award Number: **W81XWH-08-1-0583**

TITLE: **Multimodal Imaging of Pathophysiological Changes and Their Role in Development of Breast Cancer Brain Metastasis**

PRINCIPAL INVESTIGATOR: **Dawen Zhao, M.D., Ph.D.**

CONTRACTING ORGANIZATION: **University of Texas**
Dallas, TX 75390

REPORT DATE: **September 2010**

TYPE OF REPORT: **Annual**

PREPARED FOR: U.S. Army Medical Research and Materiel Command
Fort Detrick, Maryland 21702-5012

REPORT DOCUMENTATION PAGE

Form Approved
OMB No. 0704-0188

1. REPORT DATE *(DD-MM-YYYY)*	**2. REPORT TYPE**	**3. DATES COVERED** *(From - To)*
01-09-2010	Annual	1 SEP 2009-31 AUG 2010

4. TITLE AND SUBTITLE
MULTIMODAL IMAGING OF PATHOPHYSIOLOGICAL CHANGES AND THEIR ROLE IN DEVELOPMENT OF BREAST CANCER BRAIN METASTASIS

5a. CONTRACT NUMBER

5b. GRANT NUMBER
W81XWH-08-1-0583

5c. PROGRAM ELEMENT NUMBER

6. AUTHOR(S)
DAWEN ZHAO

email: dawen.sZhao@utsouthwestern.edu

5d. PROJECT NUMBER

5e. TASK NUMBER

5f. WORK UNIT NUMBER

7. PERFORMING ORGANIZATION NAME(S) AND ADDRESS(ES) AND ADDRESS(ES)
University of Texas
Dallas, TX 75390

8. PERFORMING ORGANIZATION REPORT NUMBER

9. SPONSORING / MONITORING AGENCY NAME(S) AND ADDRESS(ES)
U.S. Army Medical Research and Materiel Command
Fort Detrick, Maryland 21702-5012

10. SPONSOR/MONITOR'S ACRONYM(S)

11. SPONSOR/MONITOR'S REPORT NUMBER(S)

12. DISTRIBUTION / AVAILABILITY STATEMENT
Approved for Public Release; Distribution Unlimited

13. SUPPLEMENTARY NOTES

14. ABSTRACT Brain metastasis represents a poor prognosis and is frequently the cause of death in breast cancer patients. Tumor microcirculation and oxygenation play important roles in malignant progression and metastasis, as well as response to various therapies. Understanding of hypoxia development and its relationship with blood brain barrier (BBB) during intracranial tumor growth will be crucial for clinical management of breast cancer brain metastasis. We have developed a MRI approach based on an interleaved T2*- and T1-weighted MRI sequence, which will provide information of both tumor vascular and tissue oxygenation. Moreover, by introducing hypoxia reporter gene (HRE-luciferase) into breast tumor lines, we will be able to use bioluminescence imaging to monitor hypoxia initiation and development of intracranial tumors. We will also correlate BBB function based on dynamic contrast enhanced (DCE) MRI with tumor hypoxia. We believe that integration of MRI and BLI will provide temporal and spatial information of tumor hypoxia evolution. Tumor hypoxia leads to resistance to anticancer therapies, in particular radiation, which is perhaps the most important treatment modality in our current armamentarium for brain metastasis. A combination of radiation with hypoxia modifier, 2-methoxyestradiol, on brain metastases will be evaluated by in vivo imaging.

15. SUBJECT TERMS
Breast cancer brain metastasis, hypoxia, Magnetic resonance imaging, Optical imaging, irradiation

16. SECURITY CLASSIFICATION OF:			**17. LIMITATION OF ABSTRACT**	**18. NUMBER OF PAGES**	**19a. NAME OF RESPONSIBLE PERSON**
a. REPORT	**b. ABSTRACT**	**c. THIS PAGE**			USAMRMC
U	U	U	UU	17	**19b. TELEPHONE NUMBER** *(include area code)*

Table of Contents

Introduction:

Brain metastasis represents an important cause of morbidity and mortality. Clinically overt brain metastases occur in approximately 10 ~ 15% of patients with breast cancer (1, 2). The incidence of brain metastasis seems to have increased over the past decade, and may be the paradoxical result of effectiveness of drugs on primary breast cancer. Perhaps even more alarming are the growing numbers of breast cancer patients who die from complications related to brain metastasis, at a time when systemic disease is under good control. In part, this may be due to the fact that chemotherapeutic agents that show efficacy against systemic disease, may have poor penetration of the blood-brain barrier (BBB), which means that breast cancer metastasis in the brain may remain untreated and inaccessible to conventional chemotherapeutics (3-5).

Tumor microcirculation and oxygenation play important roles in malignant progression and metastasis, as well as response to various therapies. In particular, radiotherapy, and possibly some anticancer drugs, are less effective in hypoxic tumors (6, 7). There is little knowledge about tumor hypoxia during intracranial development of brain metastasis. We hypothesize that tumor hypoxia is major driving force for progression of breast cancer brain metastasis and represents a critical target for therapeutic strategies. Traditionally, pathophysiological and biological studies of brain tumor models involve sacrificing animals at different time points, and thus require a large number of animals. *In vivo* imaging promises greater efficiency since each animal serves as its own control and multiple time points can be examined sequentially. In addition to anatomic information, magnetic resonance imaging (MRI) has been increasingly applied to studying tumor pathophysiology. Blood Oxygenation Level Dependent (BOLD) MRI based on T_2^* contrast, deoxyhemoglobin, is sensitive to tumor vascular oxygenation. Recently, several studies have suggested a possibility of assessing tissue oxygenation by direct T_1 shortening due to oxygen molecule (8, 9). We have developed a MRI approach based on an interleaved T_2^*- and T_1-weighted sequence, which provides information of both tumor vascular and tissue oxygenation. Here, we plan to apply this new MRI approach to evaluating tumor hypoxia among various breast tumor lines growing intracranially.

Bioluminescence imaging (BLI), based on *in vivo* expression of luciferase, the light emitting enzyme of the firefly, is being rapidly adopted in cancer research. Luciferin, the substrate of luciferase, crosses the cell membrane and penetrates the intact BBB after injection in mice (10, 11). Several studies have demonstrated that the BLI is capable of tracking intracerebral neural cell migration (12) or monitoring intracranial tumor growth and its response to treatment (10), (13). Here, we propose to introduce a hypoxia reporter system, Hypoxia responsive element-luciferase (5HRE-luc), to various breast cancer cells. Hypoxia Inducible Factor-1alpha (HIF-1α) activity will be monitored via *in vivo* BLI by using a luciferase reporter gene under the regulation of an artificial HIF-1-dependent promoter, 5HRE (14, 15). Integration of MRI and BLI will provide temporal and spatial information of tumor hypoxia evolution.

Body:

The Statement of Work in this project had two major tasks:

Task 1. Establish mouse xenograft models of breast cancer brain metastasis and evaluate differential biological features among various breast cancer cell lines (Months 1-8):

During the previous periodr of the project, the model of breast cancer brain metastasis has been successfully established by intracranial inoculation of breast cancer cells. The single nodule lesion was visualized and followed up by both BLI and MRI. In addition to anatomic structure, functional MRI was applied to study

tumor vascular perfusion (perfusion-w eighted MRI) and BBB perm eability (DCE MRI) and tumor hypoxia (BOLD and TOLD).

To mimic the clinical situation, in w hich m ultiple lesions are often detected in patients of breast ca ncer brain metastasis, we have c reated a m ouse mode l to have numerous tumors in brain b y intraca rdiac (left ventricle) injection of breast cancer cells during this reported period.

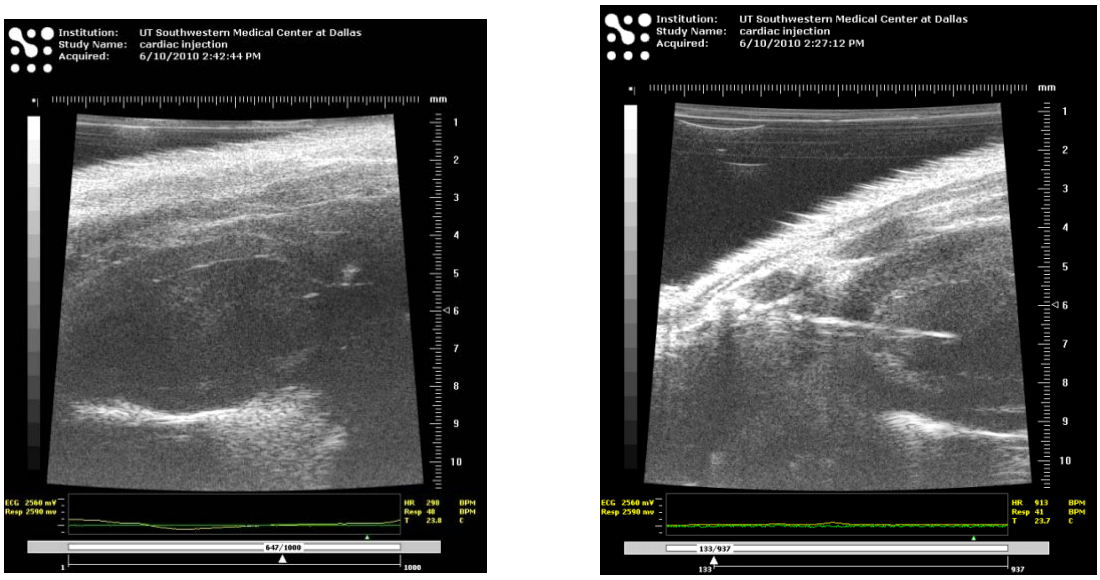

Fig. 1 Ultrasound guided intracardiac injection of human breast cancer MDA-MB-231-brain cells (obtained from Dr. Patricia Steeg).
The left ventricle of a mouse was identified by Visualsonics Vevo ultrasound system (left) and 2 x 10^5 cells in 100 μl of the serum-free medium were injected into it by using 25 G needle (right).

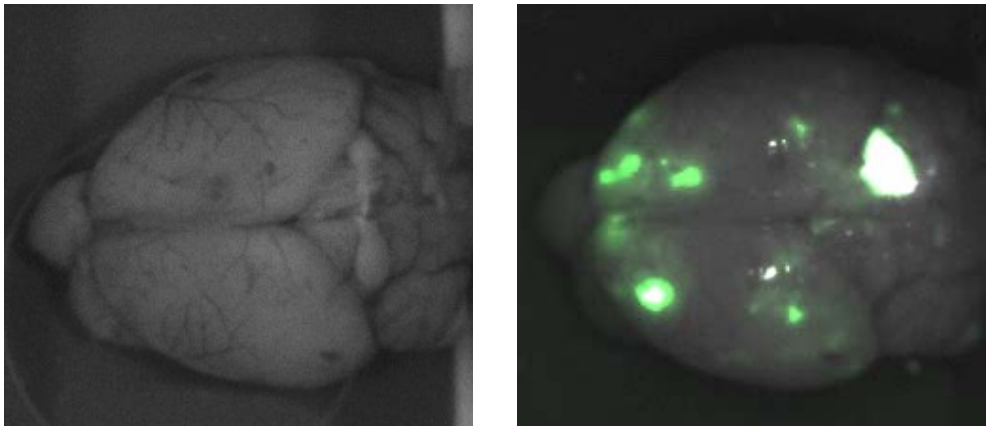

Fig. 2 A mouse model of breast cancer brain metastasis with multiple intracranial lesions. Twenty days after intracardiac injection of human breast cancer MDA-MB-231-brain-GFP cells, numerous brain lesions were visualized after the whole brain dissection by using optical imaging system. The lesions were found to distribute throughout the brain.

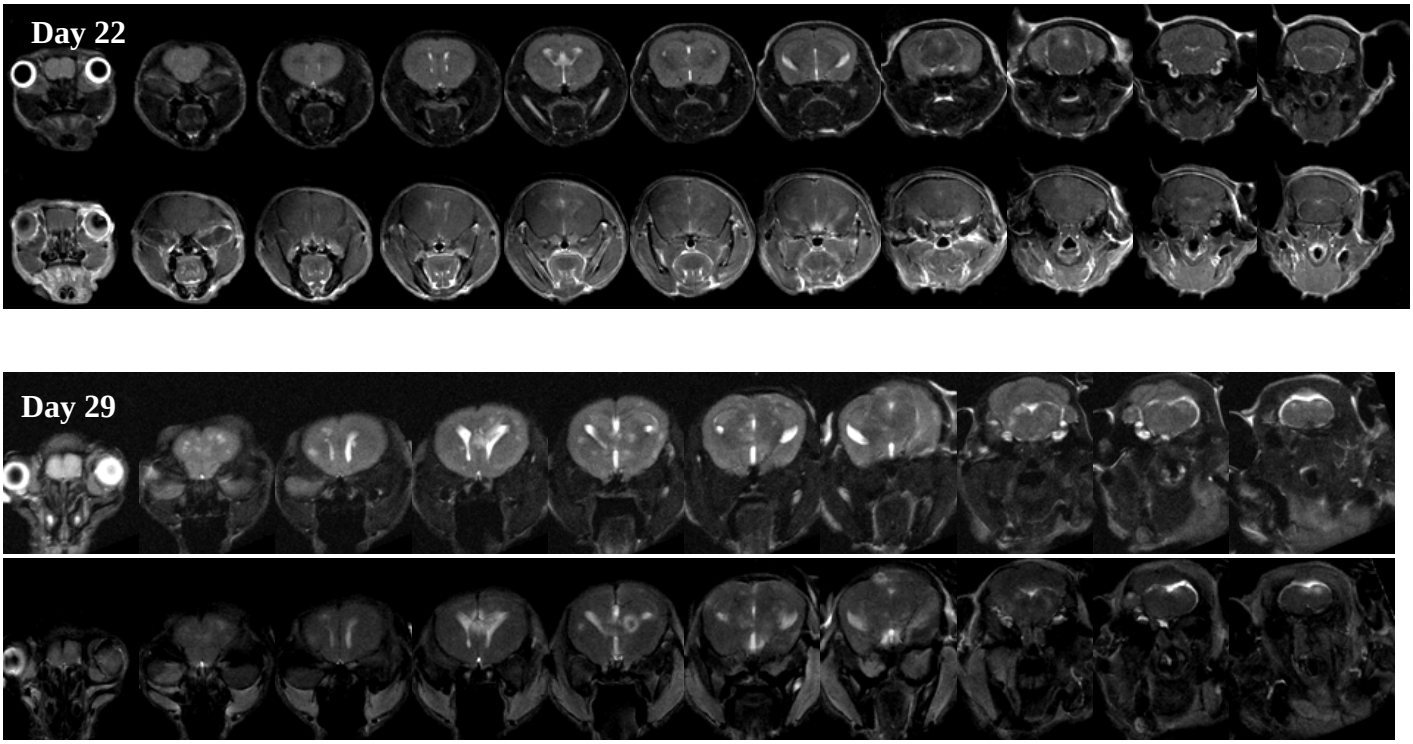

Fig. 3 MRI follow-up of the intracranial tumor growth. MRI started on Day 22 after intracardiac injection of tumor cells. Consecutive 1 mm thick MRI sections on T2- (top row) and T1-weighted contrast enhanced (bottom row) MRI showed no obvious tumor lesions. However, follow-up MRI on day 29 revealed wide spreading hyperintensity lesions from frontal lobes to posterior fossa on both T2- and T1-weighted contrast enhanced images.

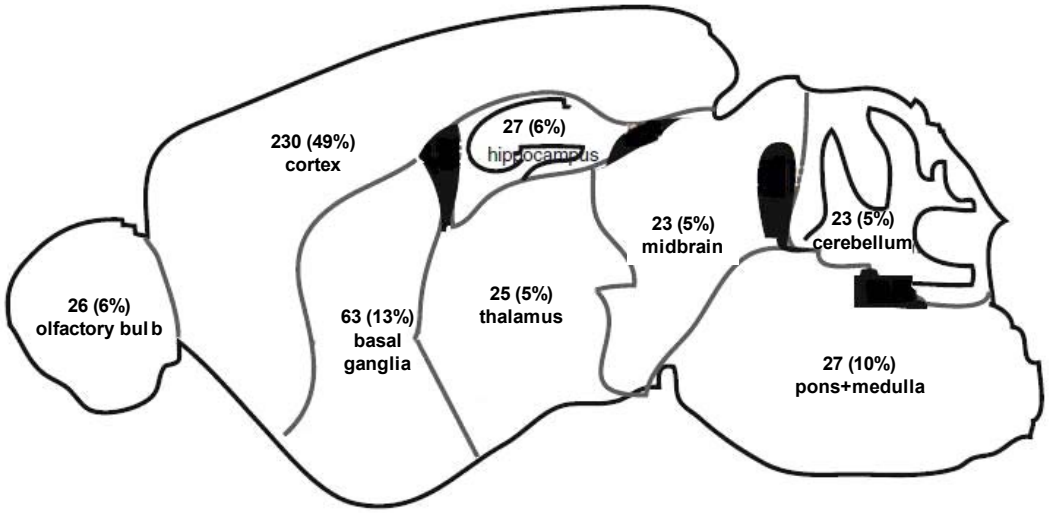

Fig. 4 Distribution of the intracranial metastases based on MRI. The total number of metastases located at different regions of mouse brain was determined on T2-weighted MRI and shown on the diagram. Metastatic lesions were found to spread widely from frontal lobe to posterior fossa.

Our data, as shown above, clearly demonstrated that the intracardiac model can produce multiple metastatic lesions, varying in tumor size. Non-invasive MRI is capable of detecting early stage of the lesions at a size as small as < 0.5 mm and followed up their growth. These intracranial metastases were found to distribute throughout the whole brain with a preferable site at cortex.

Task 2. Multimodal imaging evaluation of intracranial tumor hypoxia development and its correlation with blood brain barrier as well as aggressiveness of breast cancer brain metastasis (Months 9-24).

During the first reported period, perfusion-weighted DSC MRI was initially incorporated into this project to evaluate tumor vascular perfusion. In the current period, the technique has been implemented with improved mathematic modeling and allowing more MRI slices to be interrogated. The following graphs demonstrated the model and curve-fitting used for generation of relative cerebral blood volume, rCBVmap.

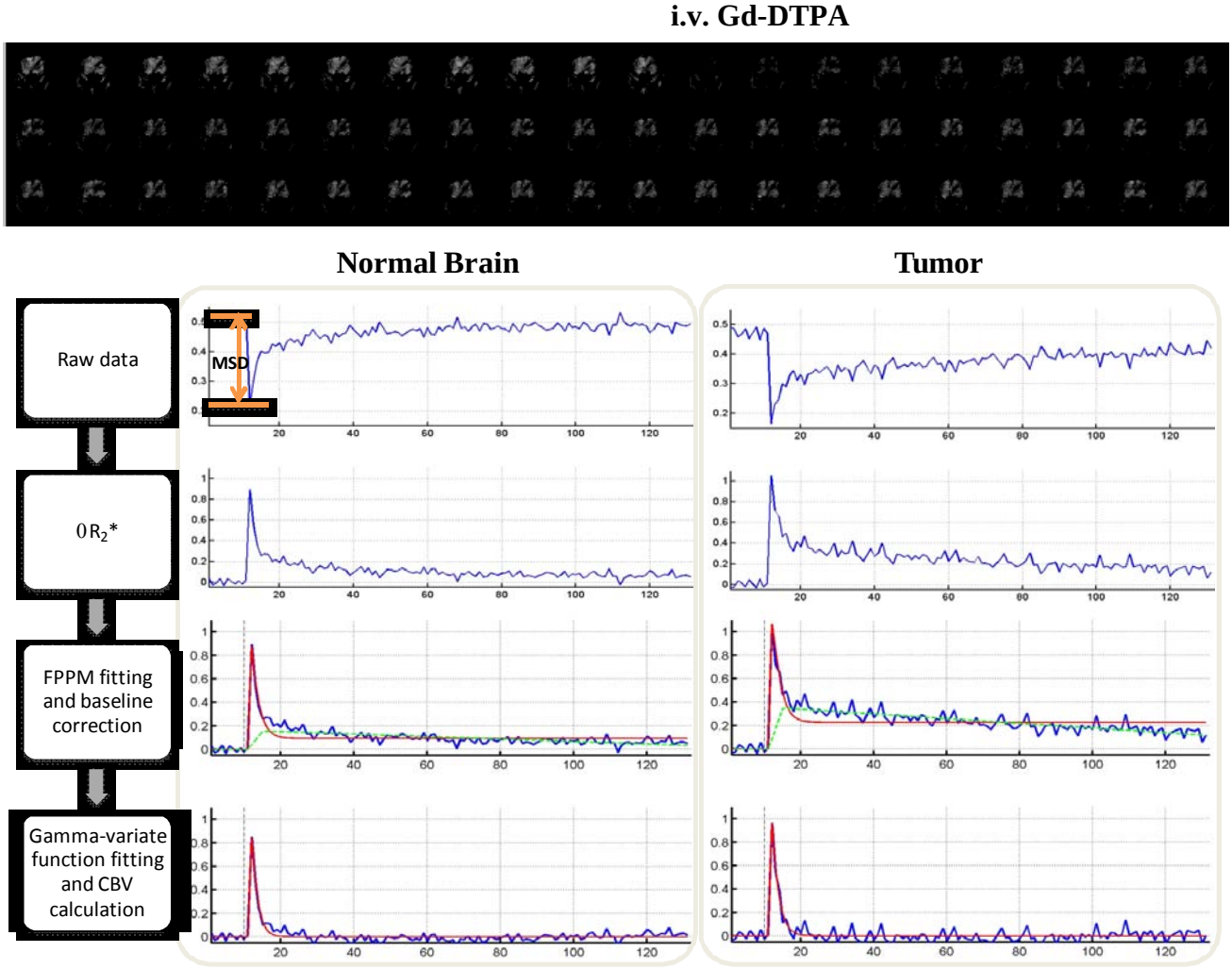

Fig. 5 ***Data analysis strategy for rCBV.***

1. Raw data time curve is extracted from DSC image series.
2. DR_2^* is calculated from raw data time curve.
3. FPPM is applied to detect the general trend of DR_2^*. Then, a three segment baseline is generated.
4. Gamma-variate fitting is applied to corrected DR_2^*, and the area under the bolus is proportion to CBV.

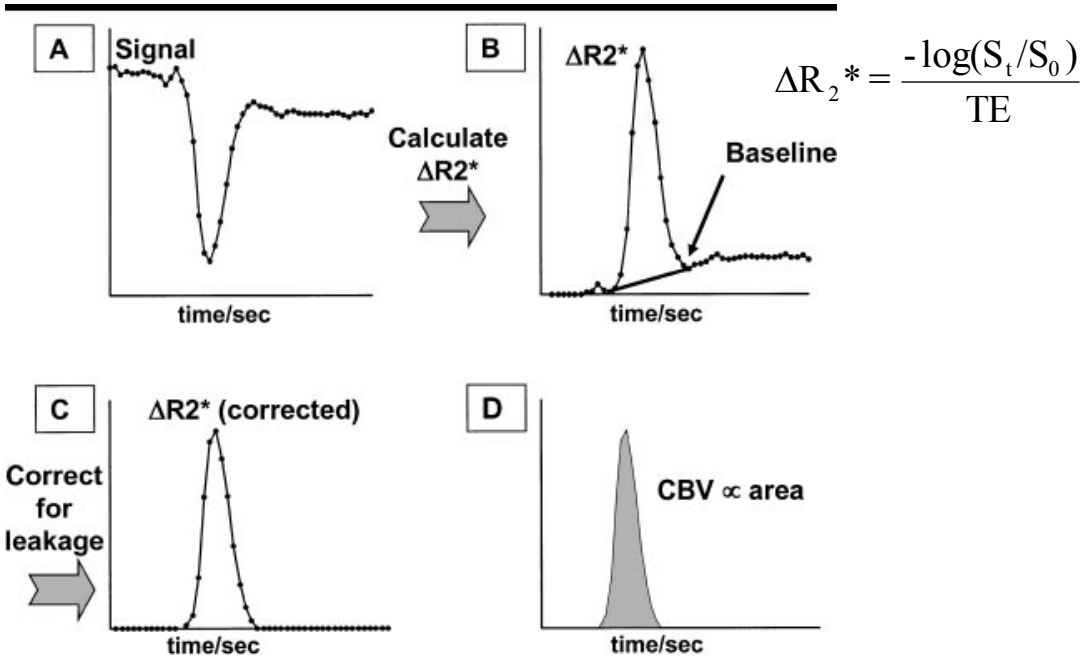

Fig. 6 Diagrams illustrate calculation of rCBV. *A, Signal intensity* decrease during passage o f contrast agent bolus is measured from a series of gradient-echo echo-planar MR images. *B, Change in the* relaxation rate (R2*) is calculated from signal intensity, and a baseline subtraction method is applied to measured data. *C, Corrected* R2* curve. *D, rCBV is proportional to the area under curve (shaded* area).

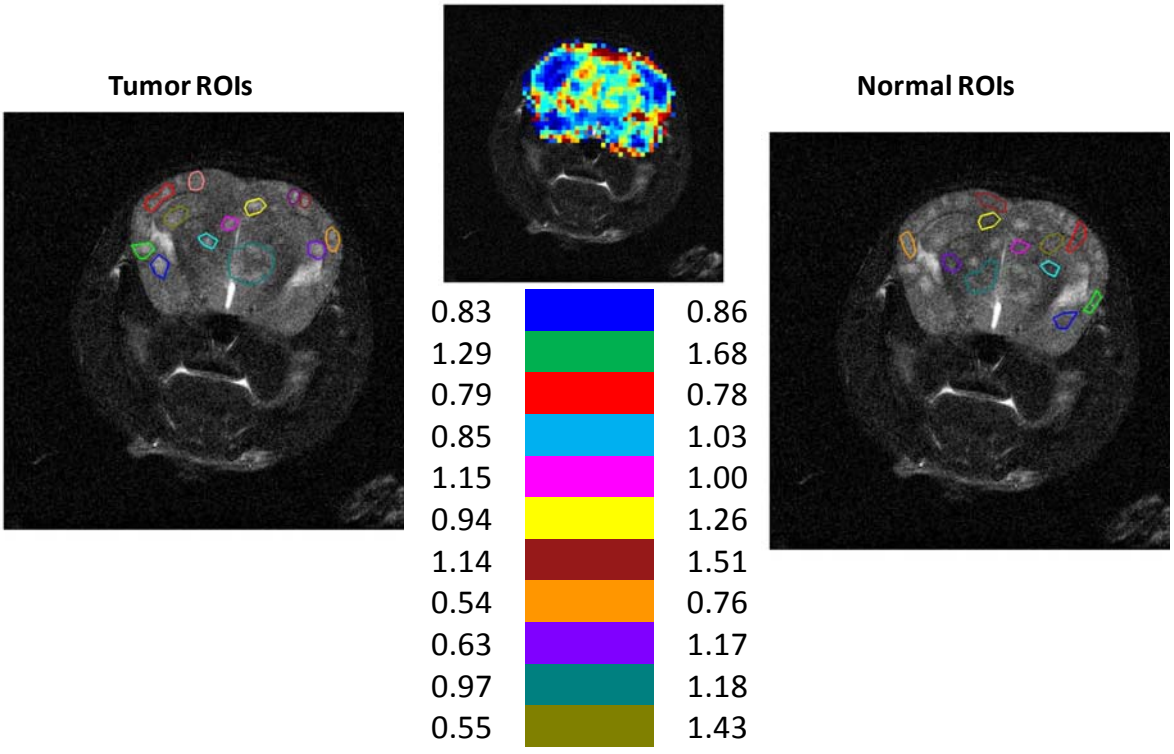

Fig. 7 Study of rCBV of breast cancer brain metastases. Left: Metastatic lesions were seen on T2-weighted MRI slice of a representative mouse brain 14 days after intracardiac injection od breast cancer MDA-MB-231-br cells. ROIs of individual tumors were outlined. Reference ROIs were selected from normal brain tissues contralateral to the tumor lesions (right). Map of rCBV was created and overlapped on the anatomic image. Values for individual ROIs of tumors and contrlateral normal brain were obtained from the map showing tumors have significantly lower rCBV (mean = 0.88 ± 0.25) than normal brain regions (mean = 1.15 ± 0.3; $p < 0.01$).

Table 2. Comparison of rCBV of tumor vs. normal brain in breast cancer brain metastases

MR Field	ROIs	Tumor Size	rCBV	p value
4.7T (n = 4)	Tumor (n = 20)	0.78 ± 0.53mm^2	0.84 ± 0.29	0.05
	Normal (n = 20)	-	1.00 ± 0.32	
9.4T (n = 4)	Tumor (n = 121)	0.50 ± 0.40mm^2	0.90 ± 0.49	0.04
	Normal (n = 121)	-	1.00 ± 0.42	

Table 3. Comparison of rCBV of metastatic lesions located between parenchyma and leptomeninges

Location	Tumor size	Tumor ROIs	Contralateral ROIs
Parenchyma (n = 79)	0.5 ± 0.4	0.8 ± 0.3	1.0 ± 0.4
Leptomeningeal (n = 62)	0.6 ± 0.5	1.0 ± 0.6	1.0 ± 0.4
P value	0.09	0.008	0.33

Metastatic lesions at brain parenchyma showed significantly more perfusion, as compared to those located at leptomeninges ($p < 0.05$), but no distinction in lesion size between the regions.

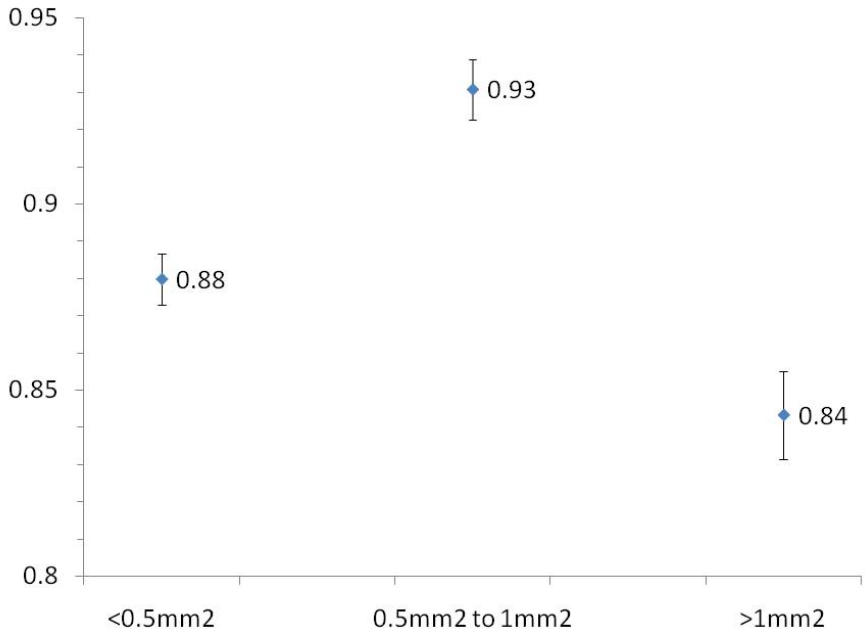

Fig. 8 Correlation between tumor rCBV and size of breast cancer brain metastases. Tumor size was measured based on the number of pixels in the ROI outlined on high resolution T_2 weighted images. Tumor sizes were separated into three groups: 1) smaller than 0.5mm^2, n=79, mean rCBV=0.88±0.54; 2) between 0.5 and 1mm^2, n=45, mean rCBV=0.93±0.37; 3) bigger than 1mm^2, n=17, mean rCBV=0.84±0.25. Standard error was plotted in the graph. No significant differences were found between these three groups.

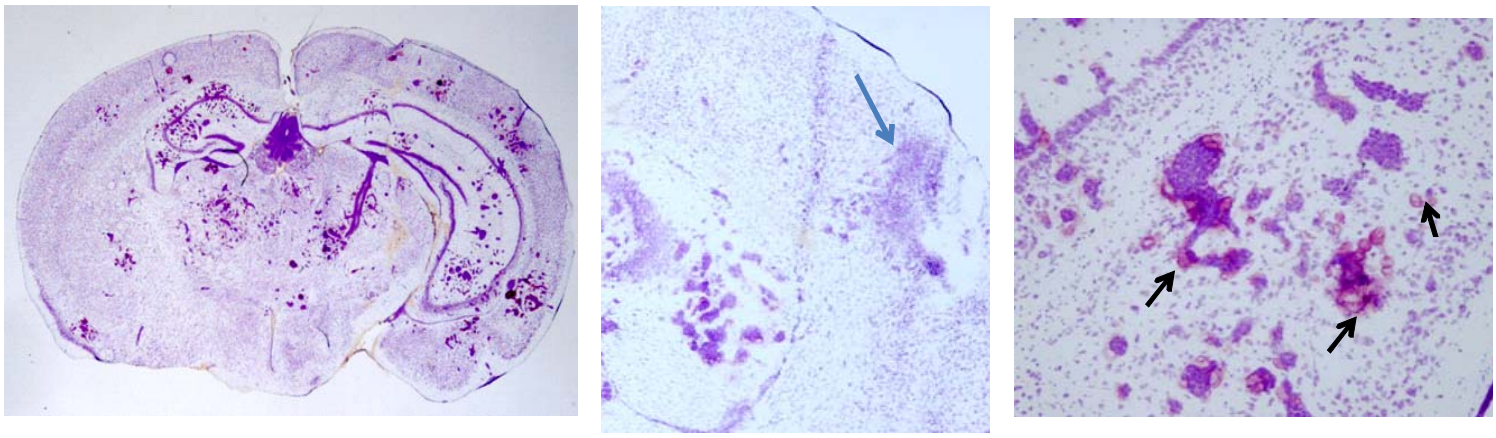

Fig. 9 Differential vascular structures between leptomeningeal and parenchymal metastases. **Left:** H&E staining of a whole mount brain section revealed numerous lesions varied in size and location. **Middle and Right:** Enlargement of a region of leptomeninges (middle) and parenchyma (right) showed peritumoral development of angiogenic vessels in parenchymal lesions (arrows, right), whereas no marked neovasculature observed in the leptomeningeal lesion (arrow, middle).

Table 3 Comparison of tumor vascular perfusion betw een the i ntracardiac brain metastatic model and intracranial implants of glioma or breast cancer model.

Tumor models	Cell line	ROI	rCBV
Intracranial implant	U87-luc	Tumor	2.86±1.75
		Normal	1.00±0.63
	MDA-MB-231/5HRE-ODD-luc	Tumor	1.57
		Contralateral	1.00
Intracardiac inject	MDA-MB-231/BR-GFP	Tumor	0.84±0.29
		Normal	1.00±0.32

In conclusion, significantl y low er rCBV values w ere ob served for brain metastases than contralateral normal b rain ($p < 0.05$; Table 2). In contra st, a parall el study of gliomblastoma by us found th at GBM has significantly higher rCBV than contralateral normal bra in. This finding, if confirmed, ma y ha ve diagnostic value in terms of differential diagnosis betw een primary brain tumor and meta stases. Moreover, rCBV of the metastases located in leptomeni ngeal regions had significantly higher values than those of parenchema ($p < 0.01$; Table 3). This ma y result from differential vascular development bet ween these regions, of which parench ymal lesions showed perit umoral formation of neovasculature at very earl y stage, w hile no distinct angiogenesis was seen for those leptomeningeal lesions. Our data also sug gest no sig nificant correlation between the size of metastases and rCBV (Fig. 8).

b. Continuing *in vivo* st udies of tu mor hypoxi a. 5 x 10^4 MDA-MB231-HRE-ODD-luc cells were directly inje cted into caudal nucle ar area of right side mouse brain. BLI was applied to monitoring temporal development of intratumoral hypoxia.

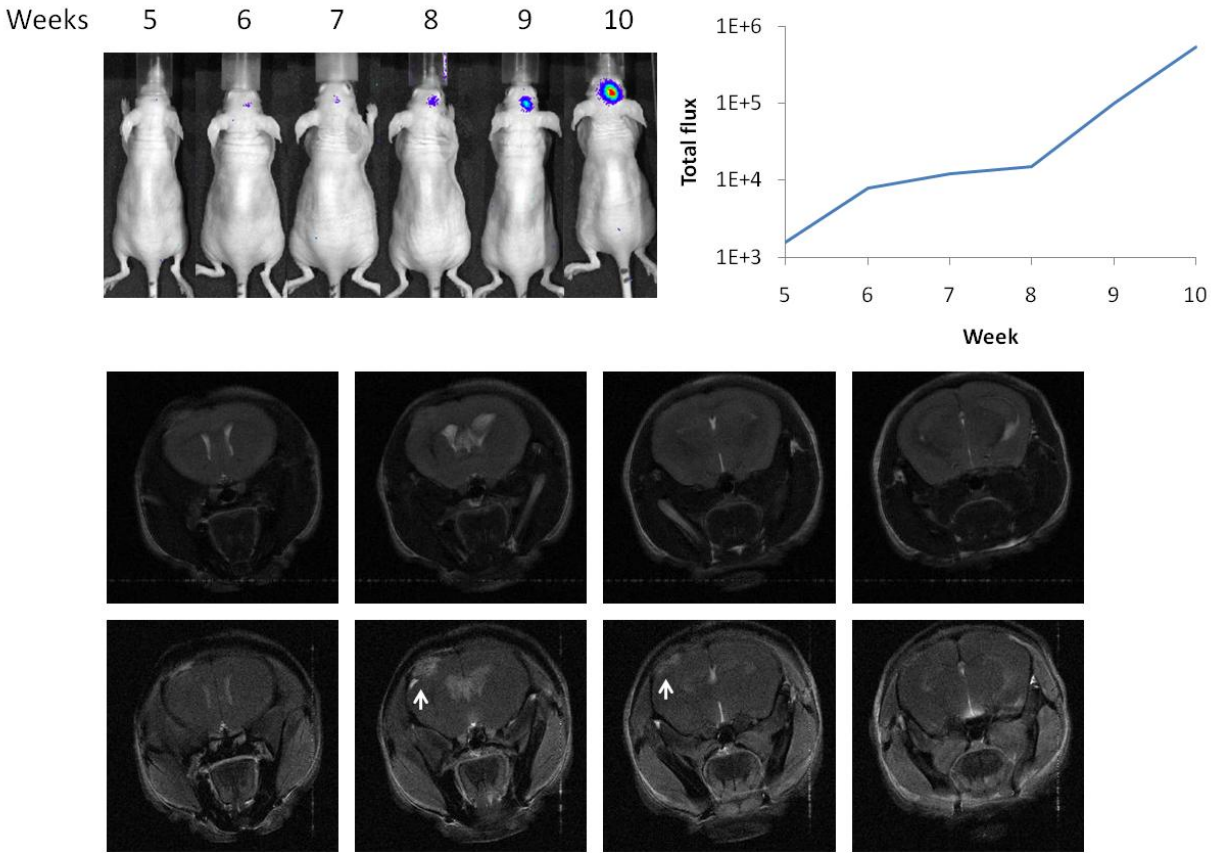

Fig. 10 *In vivo* detection of evolution of tumor hypoxia in MDA-MB231 cells with stable HRE-ODD-luc transfection. 50K cells were injected into the right side brain of a nude mouse. A week signal was found 6 wks post implantation, whic h increased in light in tensity in follow-up studies. A series of MRI T2-weighted images confirmed an intracranial tumor (arrows).

Table 4. BOLD and TOLD MRI study of tumor hypoxia

Tumor models	Cell line	ROI	BOLD (%)	TOLD (%)
Intracranial implant	U87-luc	Tumor	5.23±5.95	5.31±4.16
		Normal	2.34±2.98	5.67±5.00
	MDA-MB-231/5HRE-ODD-luc	Tumor	1.63±1.56	5.71±3.16
		Contralateral	-2.34±2.06	6.01±3.30
Intracardiac inject	MDA-MB-231/BR-GFP	Tumor	Na	Na
		Normal	Na	Na

The major goal of this project is to integrate multiple parameters of tumor hypoxia and vasculature acquired by multimodal imaging to correlate with tumor aggressiveness and understand pathophysiological mechanism underlying the clinical benefits from antiangiogenic treatment. Thus, in addition to anatomic MRI, functional MRI of studying tumor vascular and tissue oxygenation and its correlation with tumor perfusion has been initiated. Interleaved T1-weighted (TOLD) and T2*-weighted (BOLD) sequence was used to assess tumor hypoxia. Dynamic susceptibility contrast (DSC) sequence was applied to study tumor perfusion (relative tumor blood volume, rTBV). More importantly, spatial correlation between TOLD, BOLD and rTBV was performed (Figs 9 and 10).

Key Research Accomplishments

- **Establishment of a new mouse model of model breast cancer brain metastasis to mimic clinical situation.**
- **Successful application of in vivo BLI and MRI to study intracranial metastases distribution and monitoring their growth.**
- **Implement functional MRI of measuring tumor vascular perfusion rCBV.**
- **Data of rCBV show significantly lower rCBV values in brain metastases than contralateral normal brain. This finding, if confirmed, may have diagnostic value in terms of differential diagnosis between primary brain tumor and metastases.**
- **Moreover, rCBVs of the metastases located in leptomeningeal regions are significantly higher than those at parenchema ($p < 0.01$; Table 3). This may implicate differential vascular structure.**
- **Histological studies confirmed the difference in vascular development between parenchemal and leptomeningeal lesions.**
- **In vivo assessment of tumor hypoxia by BLI monitoring of the hypoxia reporter gene, HIF-1 promoted luciferase expression.**
- **In vivo MRI study of tumor oxygenation (BOLD and TOLD MRI) and correlate with tumor perfusion.**
- **Spatial correlation between these MRI parameters is performed.**

Technique problem

4.7 T MRI system, proposed to use in this project, has been under console upgrade. The machine has been unavailable for operation since this last may, which is supposed to resume soon.

Reportable Outcomes

Abstract (Published Conference Proceedings):

1) Heling Zhou, Amyn Habib, Peter Antich, Ralph P. Mason, Dawen Zhao. In vivo Imaging of Tumor Hypoxia and Vasculature of Orthotopic Mouse Brain Tumor Models. Journal of Nuclear Medicine, Vol. 51, p830, 2010.

Employment or research opportunity:

The PhD student and research assistant, Heling Zhou, continues to work on this project.

Conclusion:

During the second year of this project, we have established a new mouse model of breast cancer brain metastases. Multiple intracranial tumor lesions can be achieved using this intracardiac model. Non-invasive BLI and MRI have been performed for early detection and tumor follow up. Interesting results of in vivo imaging suggest characteristic vascular perfusion in these brain metastases, which may provide useful information to facilitate differential diagnosis. Taken together, the first and second year research has built a strong foundation for further evaluation of tumor response to therapeutics.

References:

1. Chang EL, Lo S. Diagnosis and management of central nervous system metastases from breast cancer. Oncologist 2003; 8: 398-410.
2. Gaspar L, Scott C, Rotman M, et al. Recursive partitioning analysis (RPA) of prognostic factors in three Radiation Therapy Oncology Group (RTOG) brain metastases trials. Int J Radiat Oncol Biol Phys 1997; 37: 745-51.
3. Subramanian A, Harris A, Piggott K, Shieff C, Bradford R. Metastasis to and from the central nervous system--the 'relatively protected site'. Lancet Oncol 2002; 3: 498-507.
4. Begley DJ. Delivery of therapeutic agents to the central nervous system: the problems and the possibilities. Pharmacol Ther 2004; 104: 29-45.
5. Doolittle ND, Abrey LE, Bleyer WA, et al. New frontiers in translational research in neuro-oncology and the blood-brain barrier: report of the tenth annual Blood-Brain Barrier Disruption Consortium Meeting. Clin Cancer Res 2005; 11: 421-8.
6. Brown JM, Wilson WR. Exploiting tumour hypoxia in cancer treatment. Nat Rev Cancer 2004; 4: 437-47.
7. Höckel M, Vaupel P. Tumor hypoxia: Definitions and current clinical, biologic, and molecular aspects. J Natl Cancer Inst 2001; 93: 266-76.
8. Matsumoto K, Bernardo M, Subramanian S, et al. MR assessment of changes of tumor in response to hyperbaric oxygen treatment. Magn Reson Med 2006; 56: 240-6.
9. Matsumoto S, Utsumi H, Aravalluvan T, et al. Influence of proton T1 on oxymetry using Overhauser enhanced magnetic resonance imaging. Magn Reson Med 2005; 54: 213-7.
10. Rehemtulla A, Stegman LD, Cardozo SJ, et al. Rapid and quantitative assessment of cancer treatment response using in vivo bioluminescence imaging. Neoplasia 2000; 2: 491-5.
11. Lipshutz GS, Gruber CA, Cao Y, Hardy J, Contag CH, Gaensler KM. In utero delivery of adeno-associated viral vectors: intraperitoneal gene transfer produces long-term expression. Mol Ther 2001; 3: 284-92.
12. Shah K, Bureau E, Kim DE, et al. Glioma therapy and real-time imaging of neural precursor cell migration and tumor regression. Ann Neurol 2005; 57: 34-41.
13. Jenkins DE, Hornig YS, Oei Y, Dusich J, Purchio T. Bioluminescent human breast cancer cell lines that permit rapid and sensitive in vivo detection of mammary tumors and multiple metastases in immune deficient mice. Breast Cancer Res 2005; 7: R444-54.
14. Harada H, Kizaka-Kondoh S, Hiraoka M. Optical imaging of tumor hypoxia and evaluation of efficacy of a hypoxia-targeting drug in living animals. Mol Imaging 2005; 4: 182-93.
15. Harada H, Kizaka-Kondoh S, Hiraoka M. Mechanism of hypoxia-specific cytotoxicity of procaspase-3 fused with a VHL-mediated protein destruction motif of HIF-1alpha containing Pro564. FEBS Lett 2006; 580: 5718-22.

Appendices

Objectives: Senile Plaques (SPs) and neurofibrillary tangles (NFTs) are two major neuropathological hallmarks in Alzheimer's Disease (AD).The development of new imaging agents for SPs in vivo will play an important role in clinical prediagnosis and the evaluation of clinical treatment. In this work, two series of indole and pyrole derivatives were designed and prepared as new candidate radiotracers aiming at imaging amyloid plaques in AD brain in vivo. **Methods:** Six indole derivatives were synthesized according to the Fisher-indole-reaction from corresponding phenylhydrazine and 1-(4-aminophenyl) ethanone. Four asymmetric 2. 5-diphenylpyrole derivatives were prepared by Suzuki Reaction from Boc-Protected pyrole. Considering the similar chemical structure of IMPY and the new synthesized compounds, [^{125}I]IMPY was selected as standard to measure the following compounds (IN-2, IN-3, IN-5, IN-6, PY-2, PY-3, PY-4)' affinity to β-amyloid plaques by $A\beta_{1-42}$ aggregates. **Results:** Six indole derivatives and four pyrole derivatives were synthesized successfully. Based on the potential possibility of C-11 labelling, seven Methyl-substituted compounds in aniline-N or pyrole-N were performed with measurement of Ki value. The compounds with double methylation in aniline-N display higher affinity than those with single methylation (IN-3 *vs*.IN-2; IN-6 *vs*.IN-5; PY-3 *vs*.PY-2). Methylation in indole-N or pyrole-N ring reduces the affinity to $A\beta_{1-42}$ aggregates (IN-5 *vs*.IN-2; IN-6 *vs*.IN-3; PY-4 *vs*.PY-3). The dimethylamino-carried compounds with 2-phenylpyrole ring display the higher affinity to amyloid aggregates than those with indole ring (PY-3 *vs*.IN-3; PY-4 *vs*.In-6). **Conclusions:** The experimental results indicate that In-3, PY-3 and PY-4 have the potential to develop ^{11}C-labelled radiotracers for imaging amyloid plaques in AD brain in vivo.

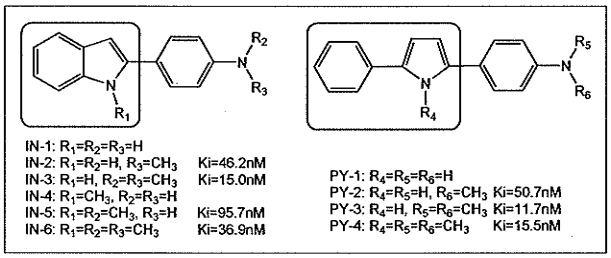

10***

***In vivo* imaging of tumor hypoxia and vasculature of orthotopic mouse brain tumor models.** H. Zhou[1], D. Zhao[2], H. Amyn[2], R. Mason[2]; 1. The University of Texas Southwestern Medical,Center, Dallas, Texas; 2. The University of Texas Southwestern Medical Center, Dallas, Texas

Objectives: Malignant brain tumors originating from the brain itself or metastases from breast tumor cells are associated with high morbidity and mortality. Monitoring tumor microcirculation and oxygenation during intracranial development of brain tumors is critical as they play important roles in malignant progression. In addition, hypoxic tumors are more resistant to radiotherapy and other anticancer drugs. We have developed orthotopic brain tumor models of glioma and breast cancer brain metastasis in athymic mice. Here, we are utilizing these models to study interplay of tumor oxygenation and vascular perfusion by applying in vivo imaging approaches.

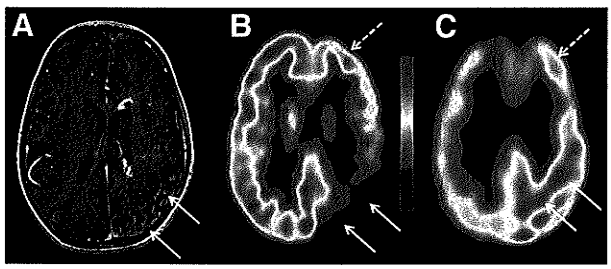

Co-registered T1 postgadolinium MRI (A), FDG PET (B) and L-[1-^{11}C]leucine (LEU) PET (C) images of one of the patients with left hemispheric angioma in the temporo-parieto-occipital region. The angioma region (solid arrow) was hypometabolic but showed increased LEU uptake. The angioma did not extend to frontal cortex; however, this region was also mildly hypometabolic (dashed arrow) and showed moderately increased LEU uptake compared to the contralateral homotopic area.

***Travel award sponsored by the Society for Molecular Imaging.

Methods: Human glioma U87-luc cells and breast cancer MDA-MB-231 cells stably transfected with the hypoxia reporter gene, HRE-ODD-luc were used. 5 x 10^4 U87-luc cells or 1 x 10^5 MDA-MB-231/5HRE-ODD-LUC cells were injected directly into the right caudal nucleus of mouse brain. Bioluminescent imaging (BLI) was used to monitor tumor growth in U87-luc glioma or hypoxia development in MDA-MB-231-HRE-ODD-luc tumors. T_2-weighted and T_1-contrast MR images were acquired to assess tumor volume. Tumor oxygenation was evaluated by Blood Oxygen Level Dependent (BOLD) and Tissue Oxygen Level Dependent (TOLD) MRI. Tumor vascular perfusion and relative regional cerebral blood volume (rCBV) was calculated based on first pass pharmacokinetic modeling (FPPM) acquired using Dynamic Susceptibility Contrast (DSC) MRI. Spatial correlation between these MRI parameters was investigated. **Results:** There was a good agreement between BLI signal intensity and MRI measured tumor volume in U87-luc glioma. Upon oxygen challenge, significant increase in R_2*-weighed signal intensity (SI) was observed in the intracranial tumors in both U87 (mean = 5.2±2. 2 %) and MDA-MB-231 tumors (mean = 1. 6±1. 6%). In line with BOLD MRI, TOLD MRI showed significantly increased SI in both U87 (mean = 5.4 ±1. 7 %) and MDA-MB-231 tumors (mean = 6.0 ± 3. 3%). DSC MRI revealed significantly higher perfusion in tumor than contralateral normal brain in both tumor types. Strong spatial correlation between DSC, BOLD or TOLD was found in three of six U87 tumors. **Conclusions:** Multimodal imaging approaches facilitate studies of both tumor anatomy and pathophysiology of tumor microenvironment.

SECTION 2

11

Drugs for imaging Alzheimer's disease. J. Baranowska-Kortylewicz, Z. Kortylewicz, J. Nearman; University of Nebraska Medical Center, Omaha, Nebraska.

Objectives: to establish noninvasive imaging methods that will aid in validating butyrylcholinesterase (BChE) as a biomarker of Alzheimer's disease (AD) progression and response to therapy. **Methods:** A series of novel BChE inhibitors was designed, synthesized and selected for their reactivity towards BChE. New drugs were fully characterized. Radiolabeling methods for several radiohalides were established. Selected drugs were evaluated in vitro, and in vivo in normal mice (wild type control) and B6C3-g(APPswe,PSEN1dE9) 5Dbo/J transgenic mice (AD mice). **Results:** Syntheses, at the macro- and no-carrier added scale, physicochemical characterization and structure-activity studies for twelve *cyclo*Saligenyl-phosphotriesters have been completed. By varying substituents on the phenyl and carbohydrate residues, four compounds were designed that bind selectively and exclusively to BChE, either as a mixture of diastereoisomers or as their corresponding, resolved diastereoisomers. Further structural refinements provided a pair of diastereomers of which one exhibits strong and exclusive binding to BChE (IC50 = 50.1 " 1. 4 nM), whereas the second does not bind to BChE at all (IC50 >30,000 nM). All non-radioactive analogues and precursors needed for radiosyntheses of *cyclo*Saligenyl-phosphotriesters were synthesized and fully characterized. Radioactive compounds were also characterized and their strong, competitive and selective binding to BChE confirmed using electrophoresis methods. The separation of all radioactive compounds into their respective S_P and R_P diastereoisomers was also accomplished. Biodistribution and pilot nuclear imaging studies in normal (wild type) and AD mice were conducted to assist in the selection of the best candidate compounds for further studies. **Conclusions:** New reagents will be useful for longitudinal noninvasive assessment of BChE levels in Alzheimer's brain.

12

Correlation of the Ability to Perform the Activities of Daily Living (ADL) to a Density Index of Acetylcholine (ACh) Vesicular Transporters in the Striata of Women with Rett syndrome (RTT). J.R. Brašić, G. Bibat, K. Hiroto, A. Kumar, Y. Zhou, J.D. Hilton, M.B. Yablonski, A.S. Dogan; Johns Hopkins University, Baltimore, MD